ELSEVIER

Thin Solid Films 424 (2003) 130–138

thin solid films

www.elsevier.com/locate/tsf

Time evolution of Cr and N on AISI 304 steel surface during pulsed plasma ion nitriding

J.N. Feugeas[a,*], B.J. Gómez[a], G. Sánchez[b], J. Ferron[c], A. Craievich[d]

[a]*Instituto de Física Rosario (CONICET-UNR), Bv 27 de Febrero 210 Bis, 2000 Rosario, Argentina*
[b]*Instituto de Física, Universidad Federal de Porto Alegre, Porto Alegre, Brazil*
[c]*INTEC (CONICET-UNL) Güemes 3450 3000 Santa Fe, Argentina*
[d]*Institute of Physics, University of Sao Paulo, Sao Paulo, Brazil*

Abstract

Chromium concentration on steels plays an important role in ion nitriding processes. In this work, the time variation of the concentration of the elements in the near-surface region of the AISI 304 (18% of Cr) stainless steel, during pulsed ion nitriding, was studied. The techniques used were the real time and in situ X-ray diffraction by Synchrotron radiation. Auger spectroscopy, Nuclear Reaction Analysis, and Conversion Electron Mossbauer Spectroscopy. Ion nitriding was performed with a 100 Hz square wave pulsed glow discharge, with different treatment times, in an atmosphere of 80% N_2 and 20% H_2 mixture, under a total pressure of 5.6 mbar. The high Cr concentration in the near surface layers ($\sim$17 Å) and the intermediate 'S' phase formation were explained through the nitrogen ion sputtering during the ion nitriding process.

Keywords: Nitriding; X-Ray diffraction; Synchrotron radiation; Crystalline; Iron alloy; Chromium alloy

1. Introduction

Stainless steel is widely used in many industrial applications. One of the most important is in food processing and storage. In the milk industry for example, the development of machinery, transport, valves, ducts, etc., have severe requirements beyond the quality of the surface. To reduce the problem of biological contamination, the surface has to be resistant to corrosion and present minimum roughness. In addition, the mechanical demands on many parts of the mechanisms have also strict requirements related to wear and surface hardness. Stainless steels meet the first requirements very well, but they do not present favorable behavior against wear and they lack hardness in many applications. In this last aspect, efforts have been made to use different methods to modify the tribological surface properties of stainless steel, but frequently, any important improvement in the tribological properties is accompanied by a decrease in corrosion resistance [1] and an increase in surface roughness.

Some decades ago, several techniques for surface treatment based on the generation of plasmas began to be used in the surface treatment of steels. One of them is ion nitriding, which is a process in which active species of nitrogen, generated by an electric discharge out of the thermodynamic equilibrium, are absorbed on a material surface and diffused into the bulk [2].

However, studies on stainless steel ion nitriding show that under some processing conditions this method can improve wear resistance without affecting the corrosion behavior [3]. Some studies conclude that those very favorable situations have a possible explanation in the existence of an 'S' phase [4–6] in which the Cr, Fe and N are bonded in a quasi-crystalline structure with Ni participation in a metallic state. Its development as the final phase can have several advantages. In spite of a lower increment in micro-hardness, with respect to the case in which a compound layer is formed (white layer), the surface maintains the same resistance to corrosion and the same degree of smoothness.

*Corresponding author. Tel.: +54-341-485-3200; fax: +54-341-482-1772.
E-mail address: jfeugeas@agatha.unr.edu.ar (J.N. Feugeas).

0040-6090/03/$ - see front matter © 2002 Elsevier Science B.V. All rights reserved.
PII: S0040-6090(02)00912-4

Table 1
Sample identification for nitriding conditions and type of analysis performed

Sample identification	Quantity	Nitriding time	Type of analysis
S_0	3	0 (without nitriding)	Auger, NRA, CEMS
S_1	3	15 min	Auger, NRA, CEMS
S_2	3	30 min	Auger, NRA, CEMS
S_3	3	1 h	Auger, NRA, CEMS
S_4	3	2 h	Auger, NRA, CEMS
S_5	3	6 h	Auger, NRA, CEMS
S_6	1	Continuous processing	XRD (Synchrotron)

Another relevant feature of the ion nitriding of steels with high content of Cr and Ni is the enrichment in Cr and Ni of the near surface region during ion nitriding [7]. Being the layers that are virtually in contact with the plasma, its role in the process of nitrogen absorption is of crucial importance and is presented in this paper.

The evolution and changes of the developing phases and compounds have to be determined to allow full characterization of the process. In this paper we describe the surface modification of AISI 304 stainless steel by pulsed glow discharges ion nitriding. The physical conditions of the plasmas used in our experiments have been described in a previous publication [8]. We studied the near surface element evolution with the time of nitriding using Auger Spectroscopy, Nuclear Reaction Analysis (NRS), and Conversion Electron Mossbauer Spectroscopy (CEMS). In addition, we followed the kinetics of phase formation and development by an in situ and real time X-ray diffraction technique [9]. For this purpose, we used an X-ray beam source of tunable, high intensity and well-collimated synchrotron radiation that reaches the surface of the sample during the ion nitriding process itself. This working condition allowed us to follow the surface evolution of a single sample under the same ion nitriding process. This experimental work was performed in the SAXS line at the National Synchrotron Light Laboratory (LNLS), Campinas, SP, Brazil.

2. Experimental

2.1. Ion nitriding conditions

Nineteen samples of austenitic AISI 304 stainless steel [Cr (18%), Ni (8%), C (0.08%), Mn (2%), Si (1%), P (0.045%), S (0.03)] 1.5 mm thick were prepared and mechanically polished (finished with 1 μm diamond paste). Three samples were left without treatment, and five sets consisting of three samples each (15 samples) were ion nitrided with an ion nitriding reactor [8] under the same physical conditions, but with different total nitriding times: 15 min; 30 min; 1 h; 2 h and 6 h.

The last sample was ion nitrided in a reactor specially adapted to the SAXS line of the synchrotron of the LNLS [9,10] but under the same physical conditions as the ones indicated above. The description of this experimental set up is fully described in Section 2.2.2. For sample identification, in Table 1 the details of the treatment of each sample is indicated.

The ion nitriding conditions basically consisted of nitrogen plasma generation by means of a glow discharge in a 5.6 bar nitrogen–hydrogen gas mixture. The electric discharge across the gas inside the reactor was generated by a pulsed power supply. The voltage was a polarized square wave with an amplitude that may be varied from 0 to 600 V. This negative potential was applied to the metallic sample holder, with the rest of the chamber at ground potential. The frequency could be varied from 0 (DC) to 1 kHz, with a control of the ratio between the active and passive parts of each cycle of the discharge. The current discharge was permanently controlled by means of a digital meter.

In our experiments, the gas composition was a mixture of 80% of nitrogen mixed and 20% of hydrogen, being maintained inside the chamber at a constant pressure of 5.6 mbar, with an applied voltage of 400 V, a frequency of 100 Hz and with an active to passive ratio of 60–40%, respectively.

2.2. Experiment with the synchrotron

2.2.1. Reactor chamber mounting on the SAXS line

The ion nitriding plasma reactor and its mounting on the SAXS line can be seen in Figs. 1 and 2. A schematic view of the ensemble appears in Fig. 1. The photograph in Fig. 2 shows a frontal view of the chamber installed in the Synchrotron X-ray beam line during one of the experiments of ion nitriding. The reactor chamber was made of stainless steel having cylindrical geometry. The sample holder was installed at the axis of symmetry in a rotating shaft, which allowed selection of the incident X-ray angle. In our case we chose an incidence angle on the surface of the sample of 25°. The X-ray beam from the synchrotron fell onto the sample's surface just on the symmetry axis of the chamber, and perpendicular to it, after entering the chamber by traversing a 200 μm

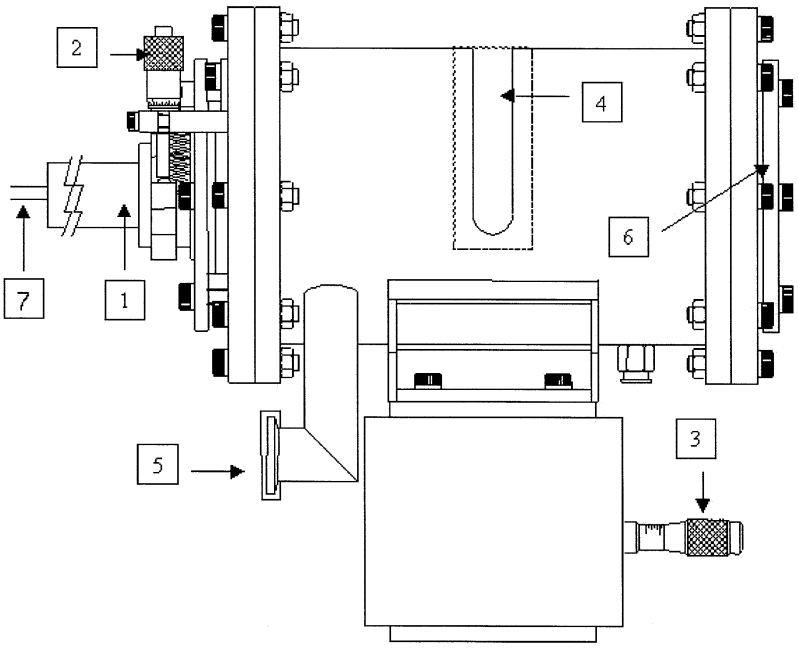

Fig. 1. Lateral view of the reaction chamber used in the experiments. The figure corresponds to a plane perpendicular to the incident X-ray beam. (1) Rotation axis. (2) Sample rotation micrometer screw. (3) Vertical displacement control (micrometer screw). (4) X-Ray diffracted exit slit (Kampton foil covered slit). (5) Vacuum pumping. (6) Glass window. (7) Thermocouple (inserted along the rotation axis).

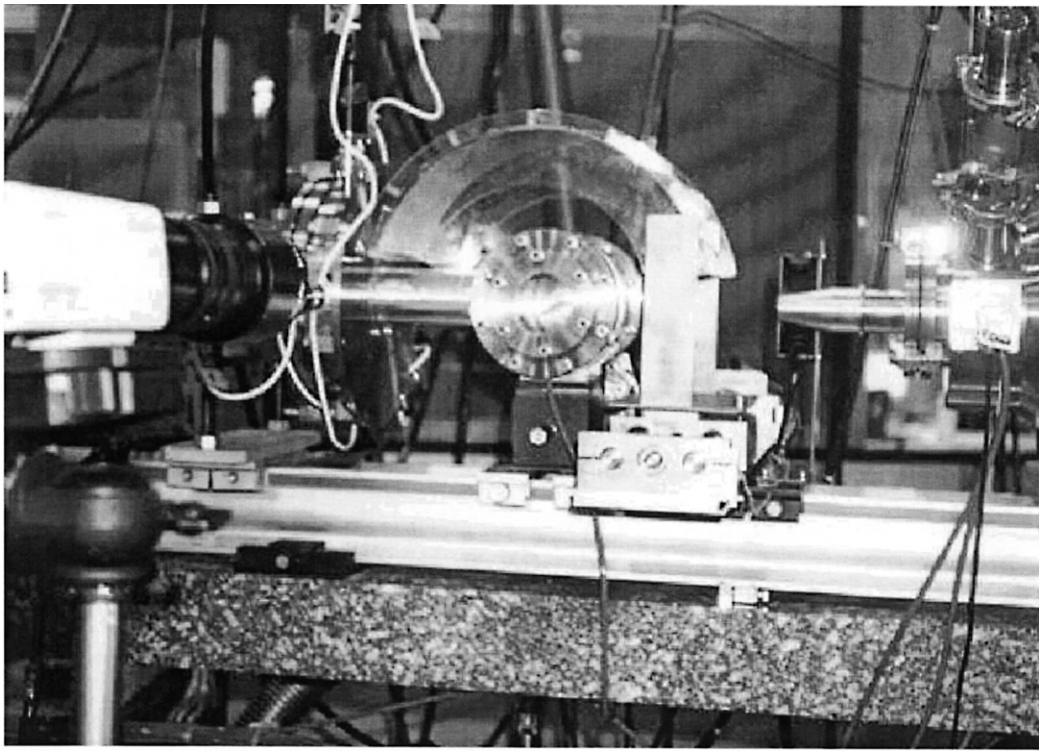

Fig. 2. Photograph showing the reaction chamber during operation. The sample is irradiated from the left. At the top, the Imaging Plate holder (concentric with the cylindrical chamber's body) can be seen.

Kapton foil window. The window is a narrow (6 mm wide) slit located along the body of the reactor covering 200° of its perimeter. This Kapton window also allows the exit of the X-rays after they are diffracted on the sample surface. Finally, the diffracted X-rays were incident (as a ~1 mm wide flux strip) onto an imaging plate (IP) located outside the chamber, fixed to a holder with the same cylindrical geometry as the chamber. A removable glass window in one of the lateral faces allowed for the loading and the visual observations of the samples during the X-ray scattering experiments.

The chamber was installed on the SAXS beam-line (see Fig. 2) of LNLS [10]. This beam-line is equipped with an asymmetric single crystal Si (111) X-ray monochromator elastically bent for horizontal focussing [11]. In our experiments we used an X-beam of 1.76 Å in wavelength. Three sets of slits collimated the beam vertically and reduced parasitic scattering. The beam cross section was typically 0.5 mm high and 1–6 mm wide at the sample position.

The vertical movement of the whole chamber for alignment purposes and the rotation of the central shaft (that fix the X-ray incidence angle α on the sample's surface) are remote controlled by stepper motors and resistive encoders. Flexible metallic bellows connect the chamber to the standard vacuum paths of the SAXS beam-line (located upstream and downstream from the sample). This connection allows for easy alignment and centering of the direct X-ray beam.

The plasma is generated as a quiescent discharge (glow discharge) inside the reactor chamber, between the cathode (sample holder and rotating shaft), and the grounded anode (chamber walls). The negatively applied voltage is a square wave with variable voltage (0–600 V), variable frequency (0–1 kHz) and variable ratio between the active and passive part of each cycle discharge. Both voltage and current were permanently monitored through an oscilloscope.

2.2.2. X-ray detection

The scattered photons in WAXS experiments were recorded by an external IP fixed to a cylindrical frame (163.8 mm diameter) concentric with the axis of the central shaft and sample holder. The frame was moved parallel to the chamber axis in such a way as to record successive X-ray scattering patterns during structural transformations. A stepping motor and a resistive encoder controlled this linear translation remotely. This IP holder is also shown in Figs. 1 and 2.

2.3. Samples characterization

The three samples without treatment (samples type S_0) and the set of three samples ion nitrided under the indicated different times of nitriding in Table 1 (S_1, S_2, S_3, S_4 and S_5), were surface characterized using three different techniques: Auger Spectroscopy, Nuclear Reaction Analysis (NRA), and Conversion Electron Mossbauer Spectroscopy (CEMS).

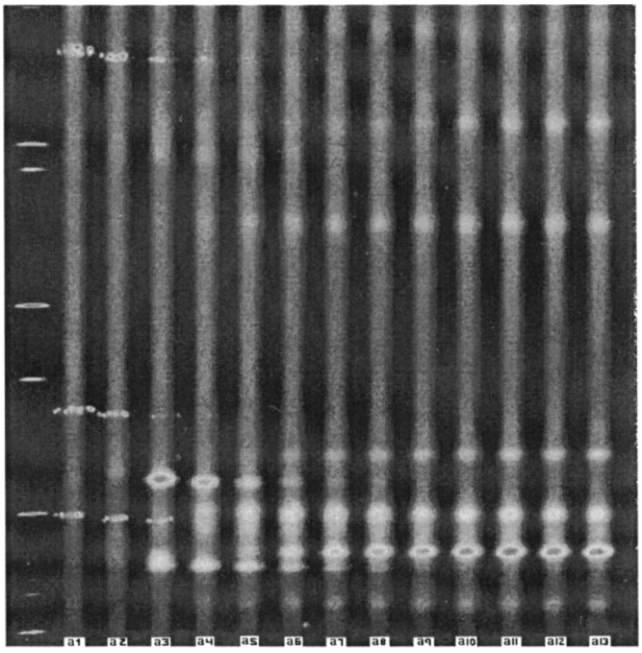

Fig. 3. Picture showing the image, recorded on the Imaging Plate, of the diffracted X-ray intensity accumulated during the time exposure, for 14 independent exposures. The first band recorded on the left corresponds to an aluminum foil calibration test. The second, moving to the right (indicated as a-1), corresponds to the non-treated AISI 304 stainless steel. The other 12 successive recordings (a-2 to a-13) correspond to the ion nitrided material after different processing times. The nitriding conditions in each case are indicated in Table 1. The different gray intensities in the picture correspond to different X-ray densities.

The last sample (S6) was characterized by real time and in situ X-ray diffraction technique (Section 2.2). In this case, the AISI 304 sample was exposed to the glow discharge under the constant physical nitriding conditions indicated above. During the process, the sample was continuously exposed to the X-ray beam from the synchrotron to obtain the successive diffractograms. The information was registered as thin sensitized strips recorded in an Imaging Plate (IP), which after being processed with a densitometer becomes the sequence of diffractograms. Fig. 3 shows the IP corresponding to the ion nitriding experiment, and Fig. 4a shows the corresponding sequence of diffractograms for 13 different moments of the nitriding process. Fig. 4b shows the first diffractogram (before the beginning of the ion nitriding process), the last and one after 40 min of ion nitriding, for purposes of clarity of phase identification. Table 2

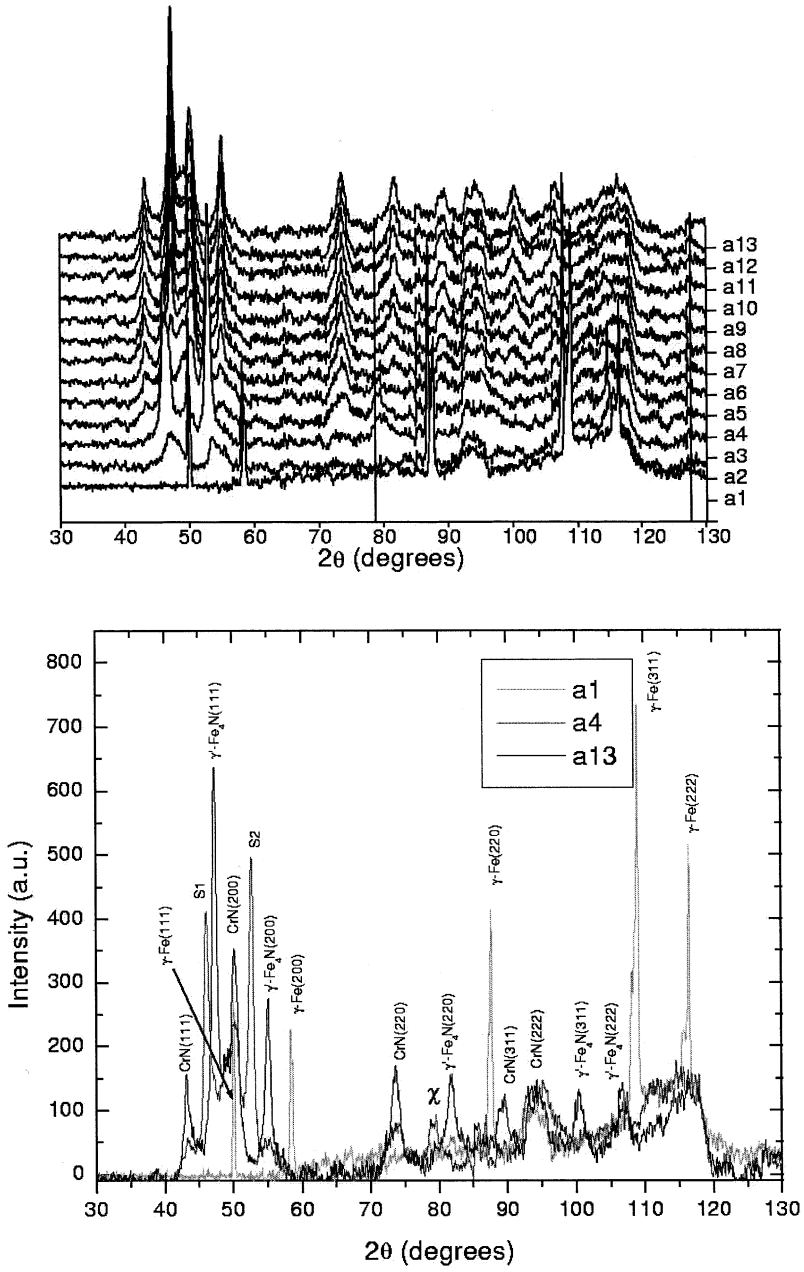

Fig. 4. (a) Sequence of diffractograms (X-ray intensity in arbitrary units vs. 2θ angle) corresponding to the IP recording. The stages of the nitriding process (a-1 to a-13) are indicated in Table 1. (b) Three diffractograms corresponding to three different stages of ion nitriding are shown for the purpose of clarity in phase identification. They correspond to the a-1, a-4 and the final stage a-13.

shows the lapse of exposure of each diffractogram during the ion nitriding process.

3. Experimental results

3.1. X-Ray diffraction analysis by synchrotron radiation

The first diffractogram showed the γ-Fe phase of the core material (a-1 in Figs. 1 and 2a,b). During the first stage of the ion nitriding process, three peaks began to develop at $2\theta \sim 46.4°$, $2\theta \sim 52.9°$ and $2\theta \sim 79.1°$ corresponding to the inter-planar distances of $d_{hkl} \sim 2.208$ Å, $d_{hkl} \sim 1.953$ Å and $d_{hkl} \sim 1.366$ Å, respectively. These phases have reached their maximum after 32 min of processing (a-4 in Fig. 4a,b) gradually decreasing and virtually disappearing after 86 min.

After 42 min of processing, the CrN and γ′-Fe_4 N phases began to appear, phases that remained up to the end of the experiment. For both f.c.c. phases the peaks corresponding to (111), (200), (220), (311) and (222)

Table 2
Data of the nitriding conditions (nitriding time sequence) for the X-ray diffraction analysis. DI is the diffractogram identification, t_i and t_f are the initial and the final time of the diffractogram exposure (the initial time of each ion nitriding process corresponds to $t_i = 00$ min), and temperature is the temperature range of the sample in the lapse of the diffractogram exposure.

DI	t_i (min)	t_f (min)	Temperature (°C)
a-1	00	10	38–254
a-2	11	21	277–365
a-3	22	32	370–396
a-4	32	42	396–400
a-5	42	52	403
a-6	53	63	404
a-7	63	73	402
a-8	75	85	404
a-9	86	96	405
a-10	96	106	405
a-11	108	118	405
a-12	120	130	406
a-13	130	140	406

crystal orientations were observed. At the end of the 2 h and 10 min of nitriding the surface was totally covered by ~60% γ'-Fe_4 N and ~40% CrN (a-13 in Fig. 4a,b).

3.2. Auger

The results obtained by Auger spectroscopy are shown in Fig. 5. In part (a), the nitrogen concentration as a function of depth for the non-treated steel and with different nitriding times are displayed. In part (b) and part (c), the same kind of plots are displayed for the chromium and iron concentrations, respectively. The Auger analyses were done at different depths by a sequence of time controlled (1 min per spectrogram) argon ion sputtering of the surface. The sputtering material removal rate could be evaluated as ~4.8 Å per min. From the results it was possible to see that the concentration profile evolution of nitrogen (bell-shaped profile) showed a maximum at ~4 min of sputtering (~4 m-s), that corresponds to a depth of ~19.2 Å. This could be seen from the very beginning of the ion nitriding process (Fig. 5a). This maximum became a plateau ~28.8 Å (~6 m-s) wide, that begun at ~19.2 Å (~4 m-s), after 6 h of ion nitriding. The maximum concentration of nitrogen was 20% after the first 15 min of treatment, becoming stabilized at a concentration of 33% after 6 h of treatment. After 6 h of ion nitriding, an almost stable nitrogen concentration profile was observed. This profile consisted in a maximum value near the surface, followed by a gradual decreasing down to a depth of ~288 Å (~60 m-s) in which a stable nitrogen concentration value of 13% was observed.

For chromium (Fig. 3b) during the first stages of the ion nitriding process (15 min) there was an important Cr concentration reduction in the first ~38.4 Å (~8 m-s) depth. This behavior was gradually reversed for higher ion nitriding times. A maximum value at ~38.4 Å (~8 m-s) was systematically observed. This maximum value continuously grew with the nitriding time, reaching a saturation value of ~30% after 6 h of ion nitriding.

On the other hand, for iron (Fig. 5c), an important concentration reduction with the ion nitriding time was observed in the layers near to the surface. The non-treated material already presents a 'valley' ~19.2 Å (~4 m-s) wide near the surface. The minimum value of Fe concentration (~35%) was observed at the surface, reaching the value corresponding to the core material (74%) at the end of the valley, i.e. ~19.2 Å deep.

The minimum value of Fe concentration began to be displaced to deeper layers with the nitriding time. For 6 h of ion nitriding a minimum value of Fe concentration of ~12% was reached in a region between ~14.4 Å and ~52.8 Å (3 and 11 m-s) depth. In this last case, the value of the Fe concentration of the bulk material was observed at a depth of ~168 Å (~35 m-s).

3.3. Nuclear reaction analysis

The nitrogen concentration profile evolution with the time of processing was also studied by the NRA method. The results, which appear in Fig. 6, showed approximately similar concentration profiles to those measured by Auger, having a maximum concentration in this case at ~100 Å for each of the nitriding times used. Through this method it was possible to see that after the maximum, the nitrogen concentration began to be gradually reduced down to a depth of ~1000 Å, where the concentration became almost constant (plateau) down to the deepest layer studied with this technique, that can be estimated to be ~2500 Å.

3.4. Conversion electron Mossbauer spectroscopy analysis

CEMS is a technique that can give information about the phases in which iron is involved. The depth involved in the analysis can be considered as ~200 nm. The CEMS spectra for the non-treated material and for the 6 h of treatment showed consistency with the use of subspectras attributed to the γ-Fe phase and Fe–Cr in the first case, and to the γ'-Fe_4N in the last one. Nevertheless, for the intermediate nitriding times there was a difficulty in the subspectra adjustment that could not be satisfactorily resolved.

4. Discussion

To explain the near surface element distribution, we have considered the sputtering effect caused by the

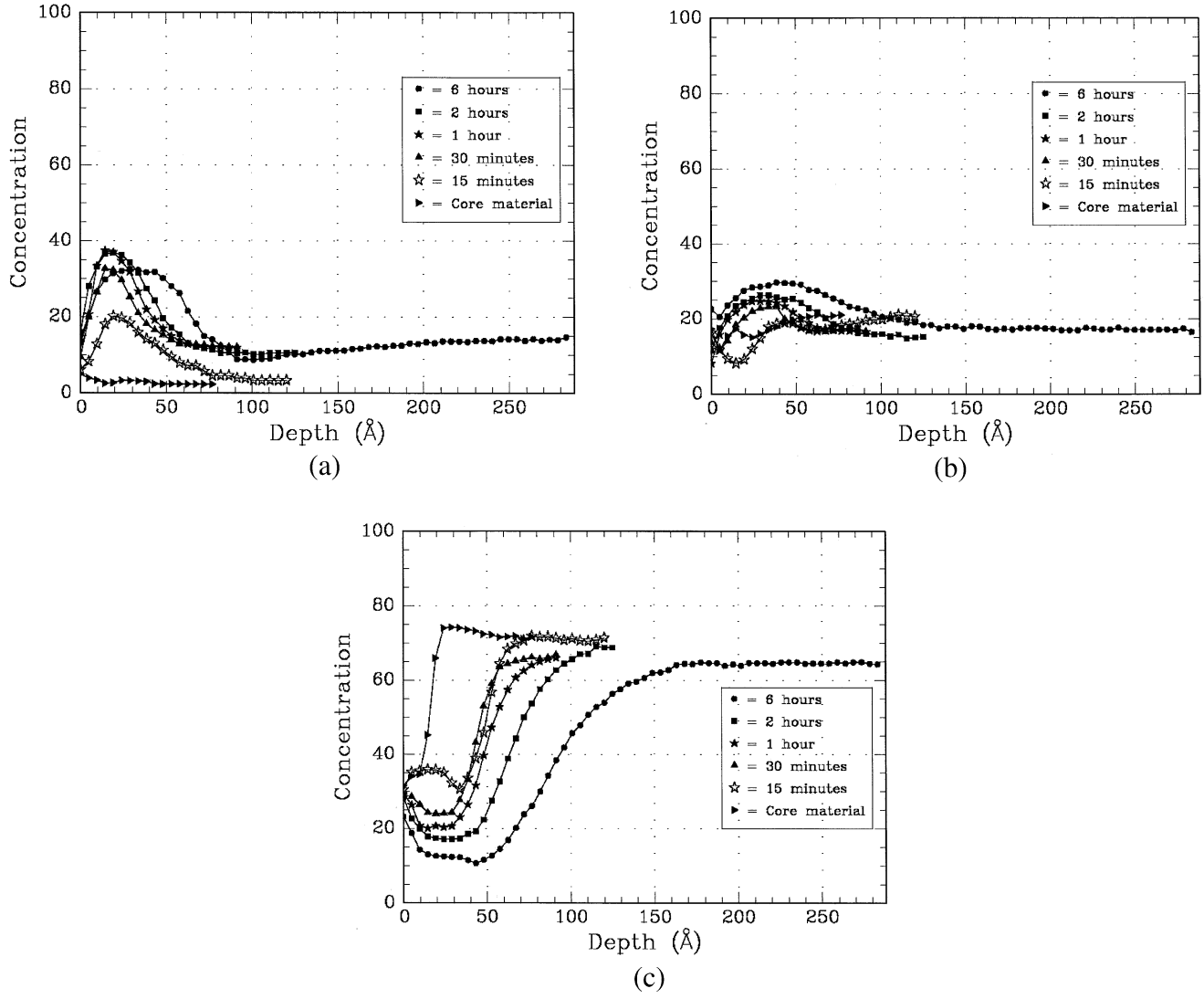

Fig. 5. Auger spectra. Concentration profile with depth, (a) for nitrogen, (b) for chromium and (c) for iron. Vertical axis: concentration in %. Horizontal axis: depth in Å (1 min of sputtering ~4.8 Å).

nitrogen ions on the steel surface during the ion nitriding process. To calculate the sputtering rate of the steel constituent elements under nitrogen ion bombardment during the ion nitriding process, we have used the SRIM code [12]. We have considered the concentration ratio of the principal components of the alloy (Fe, Cr and Ni) for which 400 eV of nitrogen ions induces an equal sputtering rate of each of them. In such a situation, we can consider that the surface composition becomes almost constant. Considering the existence of nitrogen from the ion nitriding process, the result was normalized to 100%, taking into account the measured 33% of nitrogen in the plateau between ~19.2 and ~48 Å. The results gave Fe-21%, Cr-27%, Ni-19% and N-33%. Considering that the 400 eV nitrogen ions have a range of ~17 Å in steel, this concentration ratio has to be observed in the region between the surface and ~17 Å depth (~4 m-s). The Auger results (for 6 h of ion nitriding) gave a concentration ratio at the surface of Fe-22%, Cr-22%, N-15%, and at 20 Å of Fe-13%, Cr-25% and N-33%. These results can be considered sufficiently approximated to those evaluated with SRIM calculations.

On the other hand, the results of X-ray diffraction can be considered as originating in a surface layer of ~10 μm. This thickness can be estimated from the X-ray penetration considering the wavelength (1.76 Å) and the angle of incidence on the surface (25°). We can compare the X-ray diffraction results with the deepest Auger results for large ion nitriding times. After 2 h and 20 min of ion nitriding, the surface layer was composed of approximately 60% of γ'-Fe_4N and 40% of CrN. This composition gave a stoichiometric ratio between elements of Fe-48%, Cr-20% and N-32%. The

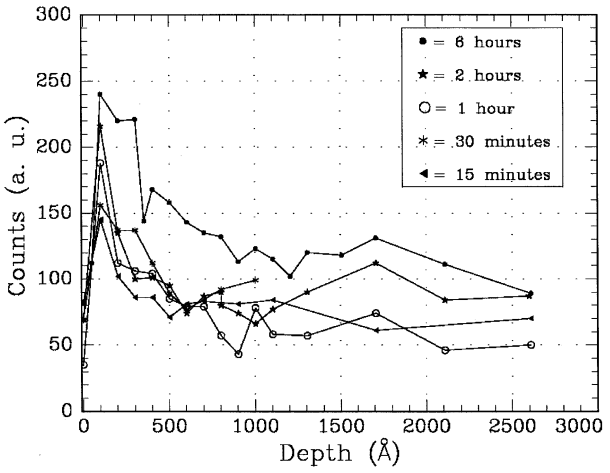

Fig. 6. Nuclear reaction analysis for nitrogen. Vertical axis; nitrogen concentration in arbitrary units (AU). Horizontal axis: depth in angstroms (Å).

Auger results at 60 m-s (~288 Å) gave the concentration ratios of Fe-65%, Cr-17% and N-12%.

The real time and in situ X-ray diffraction results showed the formation of intermediate phases, observed through the three diffraction peaks at $2\theta \sim 46.4°$, $2\theta \sim 52.9°$ and $2\theta \sim 79.1°$. The first two can be associated with the 'S' phase already reported by Menthe et al. [5] that correspond to a stoichiometry of $(Fe_4,Cr)N_2,Ni$ in which the Ni atoms are not strictly bonded to the quasi-crystalline structure. Nevertheless, the authors did not identify the third 'χ' peak. Observing our results, the S phase has a different inter-planar distance d_{hkl} for the two diffraction peaks S_1 and S_2 with respect to that observed in reference [5]. In other cases, and during the ion nitriding of DIN W Nr, 1.4882 stainless steel [13], the observed angular position of S_1 and S_2 peak variations, indicated a change in the lattice plane spacing during processing.

By observing the large profile of both peaks, it is possible that this wide structure could be the result of the superposition of the information of a large number of quasi-crystals of phase S with different inter-planar distances d_{hkl} around a mean value that in addition change with processing time. This complex behavior proved their complex quasi-crystalline nature, strongly dependent on the Cr and Ni content of the material. Otherwise, no specific conclusions could have been made with respect to the third 'χ' peak (with an inter-planar distance $d_{hkl} \sim 1.366$ Å) that accompanied the S phase in our case.

Nevertheless, the position of the three peaks strongly suggest that the two corresponding to the claimed S phase and the third called 'χ', corresponds to an f.c.c. crystalline structure. Considering that the original f.c.c. structure of the AISI 304 stainless steel and the f.c.c. structure for the final γ'-Fe_4N, we can assume that those three peaks are part of an evolution of the austenite as the nitrogen concentration increases in the matrix during the ion nitriding process.

The results (not presented in this paper) of CEMS can be justified by the initial state of the surface and the last stages of ion nitriding. Nevertheless, for the intermediate time of nitridings, no subspectras were found for a good adjustment to the Mossbauer spectra.

5. Conclusions

The well known fact that during ion nitriding of AISI 304 stainless steel the Cr concentration in the surface layers increases, can be associated with the selective nitrogen ion sputtering of the alloying elements that modify the composition until an equilibrium state is reached. In terms of Cr content, it implied an increase from the original 18% of the core material to the 25% observed (by Auger spectroscopy) in depths around the nitrogen ion range in steel, which is ~17 Å.

On the other hand, the use of the in situ and real time X-ray diffraction technique using synchrotron radiation, have proved to be an interesting technique to study the ion nitriding kinetic, because the study is concentrated on a single sample, treated under the same and non-interrupted process. The results showed intermediate phase formation that could be identified as the 'S' phase, a phase that was gradually and totally replaced by the CrN and γ'-Fe_4N phases after longer periods of ion nitriding. This intermediate state composed of the 'S' phase can be attributed to the Ni concentration increase due to the selective sputtering effect on the surface layers (that rose from 8 to ~19%), and can be considered as an expanded austenite originating in the original crystal structure of the austenitic AISI304 stainless steel. In references [14,15] for example, the authors suggest that the S-phase is a metastable nitrogen-supersaturated austenite structure called γ_N, formed by the diffusion of nitrogen atoms into the γ-Fe matrix. After a longer period of ion nitriding, the nitrogen concentration is increased in deeper layers of the material (due to the diffusion process), inducing the bonding of the nitrogen to the Cr and Fe and developing the stable CrN and γ'-Fe_4N phases, that replace definitively the 'S' phase.

Acknowledgments

Work supported by ANCYPT (PICT 12-06038), Argentina and performed under successive Research Contracts of the International Atomic Energy Agency, Vienna, Austria. The first author is a member of the Iberoamerican Program CYTED (Technology of Mate-

rials) and the South American Program NOTIMAT/MATERIA.

References

[1] J. Takada, Y. Ohizumi, H. Miyamura, H. Kuwahara, S. Kikuchi, I. Tamura, J. Mater. Sci. 21 (1986) 2493.
[2] H. Michel, T. Czerwiec, M. Gantois, D. Ablitzer, A. Ricard, Surf. Coat. Technol. 72 (1995) 103.
[3] P.A. Dearnley, A. Namvar, G.G.A. Hibberd, T. Bell, Proceedings of the First International Conference on Plasma Surface Engineering. Garmisch-Partenkirchen, 1988, DGM Informationsgesellschaft, Oberusel, 1989, 219.
[4] A. Matthews, A. Leyland, Surf. Coat. Technol. 71 (1995) 88.
[5] E. Menthe, K.T. Rie, J.W. Schultze, S. Simson, Surf. Coat. Technol. 74/75 (1995) 412.
[6] S.P. Hannula, P. Nenonen, J.P. Hirvonen, Thin Solid Films 181 (1989) 343.
[7] V.Y. Nosenko, A.L. Pivovarov, S.P. Chenakin, V.T. Cherepin, Nucl. Inst. Methods Phys. Res. B 119 (1996) 411.
[8] B.J. Gómez, S.P. Brühl, J.N. Feugeas, A. Ricard, J. Phys. D: Appl. Phys. 32 (1999) 1239.
[9] D.J. Cookson, B.A. Hunter, S.J. Kennedy, R.F.J. Garret, Synchrotron Radiat. 5 (1998) 926.
[10] J. Feugeas, J. Hermida, B.J. Gómez, G. Kellermann, A. Craievich, J. Phys. D: Appl. Phys. 32 (17) (1999) 2228.
[11] G. Kellermann, F. Vicentin, E. Tamura, M. Rocha, H. Tolentino, A. Barbosa, A. Craievich, I. Torriani, J. Appl. Crystallogr. 30 (1997) 80.
[12] SRIM (The Stopping and Range of Ions in Matter). J.F. Ziegler, J.P. Biersack (http://www.research.ibmi.com/ionbeams/SRIM/SRIMLEGL.HTM).
[13] J. Feugeas, B. Gómez, A. Craievich, to be published in Surf. Coat. Technol. 2002.
[14] C. Blawert, B.L. Mordike, G.A. Collings, K.T. Short, J. Tendys, Surf. Coat. Technol. 103/104 (1998) 240.
[15] J.M. Priest, M.J. Baldwin, M.P. Fewell, S.C. Faydon, G.A. Collins, K.T. Short, J. Tendys, Thin Solid Films 345 (1999) 113.